A QUANTITATIVE DESCRIPTION IN THREE DIMENSIONS OF OXYGEN UPTAKE BY HUMAN RED BLOOD CELLS

KIM D. VANDEGRIFF AND JOHN S. OLSON
Department of Biochemistry, Rice University, Houston, Texas 77251

ABSTRACT Oxygen uptake by human erythrocytes has been examined both experimentally and theoretically in terms of the influence of unstirred solvent layers that are adjacent to the cell surface. A one-dimensional plane sheet model has been compared with more complex spherical and cylindrical coordinate schemes. Although simpler and faster, the plane sheet algorithm is an inadequate representation when unstirred solvent layers are considered. The cylindrical disk model most closely represents the physical geometry of human red cells and is required for a quantitative analysis. In our stopped-flow rapid mixing experiments, the thickness of the unstirred solvent layer expands with time as the residual turbulence decays. This phenomenon has been quantified using a formulation based on previously developed hydrodynamic theories. An initial 10^{-4} cm unstirred layer is postulated to occur during mixing and expand rapidly with time by a $(t)^{0.5}$ function when flow stops. This formula, in combination with the three-dimensional cylinder scheme, has been used to describe quantitatively uptake time courses at various oxygen concentrations, two different external solvent viscosities, and two different internal heme concentrations.

INTRODUCTION

The initial kinetic studies of oxygen uptake by intact red blood cells were carried out by Hartridge and Roughton in 1927, and since then a large number of experimental and theoretical studies have been published. The earlier work has been reviewed by Roughton (1959), and more recent analyses have been presented by Coin and Olson (1979), Weingarden et al. (1982*a*, *b*), and Kagawa and Mochizuki (1982). The basic observation is that the rate of O_2 uptake by cells in rapid mixing experiments is ~40 times slower than that of an equivalent solution of free hemoglobin. Intracellular oxygen diffusion accounts for about half of the decrease in rate; the remainder must be due to decreased rates of external diffusion, either resistance due to the plasma membrane or to unstirred solvent layers adjacent to the cell surface (Roughton, 1959, or Coin and Olson, 1979).

The magnitude of this external diffusion effect can be estimated from the following simple boundary analysis adapted from the work of Nicolson and Roughton (1951) and Kagawa and Mochizuki (1982). The oxygen flux at the cell interface can be computed using an empirical mass transfer coefficient, γ, and the difference between the concentration in bulk solvent, $C(0)$, and the first cytoplasmic layer, $C(1)$

$$\alpha \cdot D\left(\frac{\partial C}{\partial x}\right)_{x=0} \simeq \gamma\,[C(0) - C(1)]. \qquad (1)$$

The exact definition is given on the left-hand side of Eq. 1, where α is the partition coefficient between the phase at $C(0)$ and that at $C(1)$, and D is the oxygen diffusion constant between $C(0)$ and $C(1)$. Roughton (1932) and others (most recently, Kagawa and Mochizuki, 1982) have assigned values to γ by fitting observed kinetic data to a model using Eq. 1 for the outer boundary condition. The value of γ at pH 7.4 and 25° is ~0.08 cm/s when either stopped-flow or continuous flow apparatus are used for the experimental measurements (i.e., see Kagawa and Mochizuki, 1982).

Until recently the interpretation of the small value for the mass transfer coefficient at the cell interface was controversial. This parameter can be approximated by the following expression

$$\gamma \simeq \frac{\alpha D}{\Delta x}, \qquad (2)$$

where Δx is the distance between the bulk solvent and the cell cytoplasm. In the simplest analysis, Δx can be thought of as the thickness of the cell membrane, $\sim 10^{-6}$ cm. If the diffusion constant were the same in the membrane as in solvent ($D = 2 \times 10^{-5}$ cm^2/s) and $\alpha = 1$, γ should equal 20 cm/s, a value that is ~200 times greater than that observed. Roughton offered two explanations for this discrepancy. First, oxygen diffusion through the membrane could be extremely slow. Using Eq. 2, the observed value for γ, and a partition constant of 4 (Battino et al., 1968), the diffusion constant in the membrane is calculated to be 2×10^{-8} cm^2/s. This value is unrealistic since it is roughly 100 times smaller than that measured experimentally for 0_2 diffusion in red cell membranes (Fishkoff and Vanderkooi, 1975). In the second explanation, diffusion through the membrane is roughly the same as that in solvent, but

lack of efficient stirring causes stagnant solvent layers to form adjacent to the cell surface. These layers become depleted of oxygen quickly after mixing so that the bulk of the oxygen molecules must diffuse over large distances. In this interpretation, Δx represents the thickness of these layers and can be estimated from Eq. 2 using $D = 2 \times 10^{-5}$ cm^2/s, $\alpha = 1$, and $\gamma = 0.08$ cm/s. The resultant value is 2.5 μm. Roughton originally favored the membrane resistance explanation; however, it is now clear that unstirred solvent layers account almost entirely for the small mass transfer coefficient at the cell surface. Evidence of this interpretation has been discussed in detail by Coin and Olson (1979), and more recent studies supporting this view have been presented by Huxley and Kutchai (1981 and 1983) and Weingarden et al. (1982*a*, *b*).

As pointed out by Rice (1980) and Olson (1981*b*), the consideration of stagnant layers causes two computational problems. First, the external 0_2 concentration gradients that are computed using one-dimensional models (i.e., Eqs. 1 and 2) are inadequate descriptions of the real three-dimensional situation. Second, in stopped-flow rapid mixing experiments, the efficiency of stirring decays with time. Coin and Olson (1979) addressed this problem by using a model that allowed the unstirred layer thickness to increase as the reaction proceeded. They chose an exponential function to represent this process that was based on the time course of light-scattering changes that occur when red cells are mixed with buffer in a stopped-flow apparatus. Rice (1980) has criticized this empirical approach and presented a theoretical description of stirring phenomena and its decay with time. This criticism prompted us to develop more rigorous three-dimensional models that incorporate the hydrodynamic considerations presented by Rice (1980). The corresponding sets of second-order differential equations have been integrated numerically, and the resultant time courses for oxygen uptake have been compared with those observed experimentally.

EXPERIMENTAL AND THEORETICAL METHODS

Experiments

With the exception of the data in Fig. 7, all the oxygen uptake time courses and rates represent new experiments using freshly prepared red blood cells taken from K. Vandegriff. The procedures followed were identical to those described by Coin and Olson (1979) and Olson (1981*a*). Absorbance changes were collected at two wavelengths (560 and 577 nm) in a dual wavelength stopped-flow apparatus (Dionex Corp., Sunnyvale, CA), and the difference was computed to cancel out light-scattering changes. Normalization and comparison with theoretical time courses take into account a 6-ms dead time (Coin and Olson, 1979).

Mathematical Models

Simulation of the rate of oxygen uptake by a red blood cell requires the numerical integration of two second-order partial-differential equations that contain reversible chemical reaction terms. These equations have been solved in three dimensions using spherical and cylindrical polar coordinates (Crank, 1975; Smith, 1978)

Sphere:

$$\frac{\partial(O_2)}{\partial t} = DO_2 \cdot \left[\frac{\partial^2(O_2)}{\partial r^2} + \frac{2}{r} \cdot \frac{\partial(O_2)}{\partial r}\right] - k'(O_2)(Hb) + k(HBO_2) \quad (3)$$

$$\frac{\partial(HbO_2)}{\partial t} = DHbO_2 \cdot \left[\frac{\partial^2(HbO_2)}{\partial r^2} + \frac{2}{r} \cdot \frac{\partial(HbO_2)}{\partial r}\right] + k'(O_2)(Hb) - k(HbO_2) \quad (4)$$

Cylinder:

$$\frac{\partial(O_2)}{\partial t} = DO_2 \cdot \left[\frac{\partial^2(O_2)}{\partial r^2} + \frac{1}{r} \cdot \frac{\partial(O_2)}{\partial r} + \frac{\partial^2(O_2)}{\partial z^2}\right] - k'(O_2)(Hb) + k(HbO_2) \quad (5)$$

$$\frac{\partial(HbO_2)}{\partial t} = DHbO_2 \cdot \left[\frac{\partial^2(HbO_2)}{\partial r^2} + \frac{1}{r} \cdot \frac{\partial(HbO_2)}{\partial r} + \frac{\partial^2(HbO_2)}{\partial z^2}\right] + k'(O_2)(Hb) - k(HbO_2). \quad (6)$$

Cylindrical dimensions in the r- and z-directions were selected to mimic human red cell geometry. We used a 4.18-μm radius (r) and a 0.8-μm half height (z) for the cellular disk. A sphere of equivalent volume required a 2.75-μm radius (r). The surface areas were 152 μm^2 and 95 μm^2 for the cylindrical and spherical models, respectively. The one-dimensional plane sheet model was taken without modification from the earlier work of Coin and Olson (1979).

The chemical reaction of O_2 with hemoglobin was simulated as a simple, one step binding process, which is a good approximation when diffusion is the major rate limiting process and high saturation is reached (see Coin and Olson, 1979; Kutchai, 1975; Forster, 1964). Both association (k') and dissociation (k) rates were used in the model, and the deoxyhemoglobin concentration was adjusted as saturation increased. Overall fractional saturation was computed as the volume weighted ratio of HbO_2 to total protein (see Appendix). The expected time course was computed by normalizing the calculated fractional amount of deoxyhemoglobin remaining to the 6-ms value to take into account the dead time of the stopped-flow apparatus (see Appendix). Parameters used in the computations are given in Table I.

The differential equations were solved with a modified form of an Euler predictor-corrector numerical method, which had previously been used by Moll (1969) and by Coin and Olson (1979). Separate expressions were used in the computations within the cell cytoplasm, at the cell center, at the cell-solvent interface, and within the unstirred aqueous layer external to the cell (see Appendix). A DEC VAX/VMS (Digital Equipment Corp., Marlboro, MA) computer was kindly provided for our use by Dr. F. A. Quiocho to perform the calculations.

Tests were made to determine time and space intervals for computational speed and accuracy. A 1×10^{-5} s time interval was used for the first millisecond and a 1×10^{-3} s interval was used thereafter. The latter interval was tested from 1×10^{-5} to 2×10^{-3} s with little difference in the resultant calculations. The number of interval points within the cell was varied from 10 to 40 with negligible differences. Consequently, a 25-point space interval was chosen for the sphere and a 20-point space interval was chosen for the cylinder in both the r and z directions with respective grid sizes adjusted to the particular cell geometry examined. A 0.5-μm grid size was chosen for the external solvent layer. Tests were carried out using

TABLE I
PARAMETER VALUES FOR THEORETICAL COMPUTATIONS

Reaction conditions	
(O_2) after mixing	1.25×10^{-4} M
(total heme), after mixing	2.0×10^{-5} M
Diffusion constants (Kreuzer, 1970)	
DO2 (solvent)	2.1×10^{-5} cm^2/s
DO2 (cytoplasm)	
(20 mM internal heme)	0.82×10^{-5} cm^2/s
(22 mM internal heme)	0.76×10^{-5} cm^2/s
DHb	
(20 mM internal heme)	0.74×10^{-7} cm^2/s
(22 mM internal heme)	0.67×10^{-7} cm^2/s
Rate constants (Coin and Olson, 1979) $k' = 3.0 \times 10^6$ M^{-1} s^{-1} and $k = 29$ s^{-1}	
Cell volume (Wintrobe, 1974)	88 μm^3
Grid sizes:	
Spherical model	
DR (solvent)	0.5×10^{-4} cm
DR (cell)	0.11×10^{-4} cm
Cylindrical model	
DR (solvent)	0.5×10^{-4} cm
DZ (solvent)	0.5×10^{-4} cm
DR (cell)	0.209×10^{-4} cm
DZ (cell)	0.4×10^{-5} cm

0.25 to 1-μm intervals in the extracellular phase, and there was little variation in the calculated values.

RESULTS AND DISCUSSION

Differences Between One and Three-dimensional Models

Experimental and theoretical time courses for oxygen uptake are shown in Fig. 1. The open circles represent an average of five separate experimental time courses measured under the same conditions of 0.020 mM heme and 0.125 mM O_2 after mixing and with separate red blood cell samples taken from K. Vandegriff over a 6-mo period. The concentration of red cells was chosen so that net depletion of the total extracellular oxygen concentration would not need to be considered. Each time course was the average of 4–5 measurements on the same cell sample. The error bars are within the diameter of the circles.

The theoretical time courses were computed for one-dimensional plane sheet, spherical, and cylindrical models using an unstirred layer that did not change in thickness as the reaction proceeded. The progress curves shown in Fig. 1 were computed by using various stagnant layer thicknesses, from 0 to 30 μm for each model. Initially, the oxygen concentration adjacent to the cell surface was set equal to that of bulk solvent (0.125 mM), and then the external oxygen concentration was computed as a function of time in the region between the cell surface and the outer edge of the unstirred layer using the appropriate mass

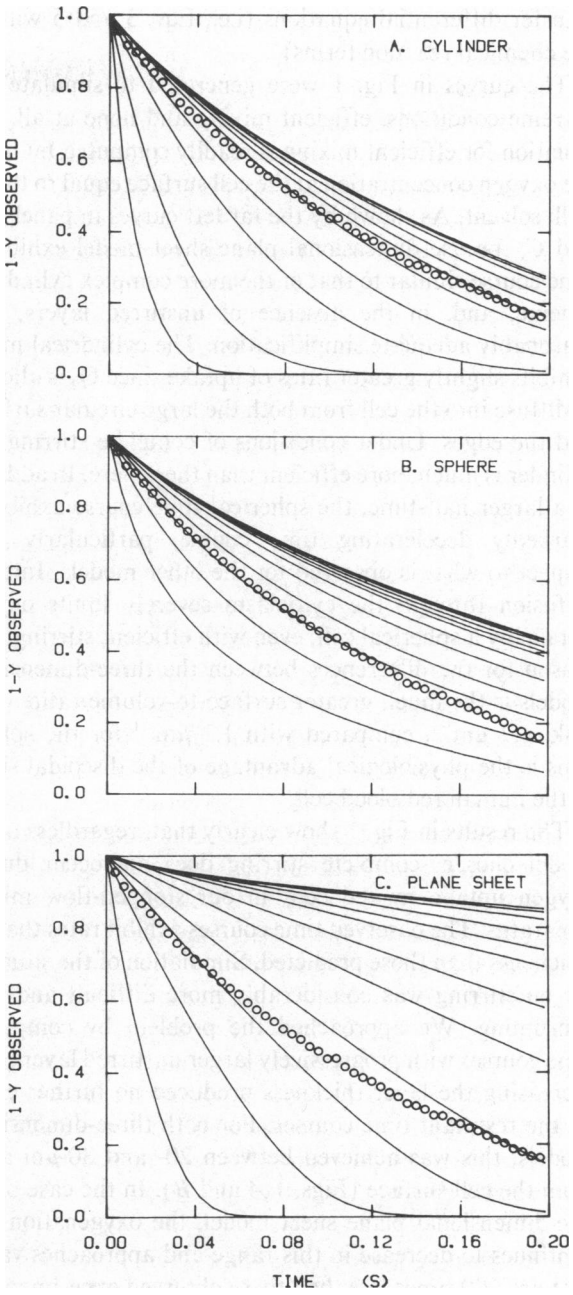

FIGURE 1 Experimental and theoretical time courses for oxygen uptake by human red blood cells. Open circles (O) represent an average of data from six separate cell preparations. The erythrocytes were taken from the same investigator (K. Vandegriff), and the internal heme concentration was 22 mM in all cases. Reaction conditions after mixing were: 0.020 mM heme and 0.125 mM O_2 in 77.5 mM NaCl, 10 μM $CaCl_2$, 58 mM NaPi at pH 7.4, 25°. Solid lines (—) represent theoretical time courses calculated using the appropriate diffusion equations with the parameters listed in Table I. (*A*) Cylindrical model time courses calculated from Eqs. 5–6 with fixed unstirred layer thicknesses of 0, 1, 3, 5, 8, 10, 12, 15, 20, 25, and 30 μm (curves go from left to right, respectively). The diffusion sublayer is extended equi-distance in the *r* and *z* directions. (*B*) Spherical model time courses calculated from Eqs. 3–4 with fixed unstirred layer thicknesses of 0, 1, 2, 3, 5, 7, 10, 12, 15, 20, 25, and 30 μm along the radial *r*-direction. (*C*) Plane sheet model time courses calculated using the algorithm described by Coin and Olson, 1979, with fixed unstirred layer thicknesses of 0, 1, 2, 3, 5, 7, 10, 12, 15, 20, 25, and 30 μm along the *x*-axis.

transfer differential equations (i.e., Eqs. 3 and 5 without the chemical reaction terms).

The curves in Fig. 1 were generated to simulate two extreme conditions, efficient mixing and none at all. The situation for efficient mixing is readily computed by fixing the oxygen concentration at the cell surface equal to that in bulk solvent. As shown by the far left curves in panels 1 *A* and *C*, the one-dimensional plane sheet model exhibits a time course similar to that of the more complex cylindrical scheme, and, in the absence of unstirred layers, is a reasonably adequate simplification. The cylindrical model exhibits slightly greater rates of uptake since O_2 is allowed to diffuse into the cell from both the large circular surfaces and the edges. Under conditions of complete stirring, the cylinder is much more efficient than the sphere. In addition to a larger half-time, the spherical time course exhibits a markedly decelerating time course, particularly with respect to what is observed for the other models. Internal diffusion through the cytoplasm severely limits oxygen uptake by a spherical cell, even with efficient stirring. The reason for the differences between the three-dimensional models is the much greater surface-to-volume ratio of the disk, 1.7 μm^{-1}, compared with 1.1 μm^{-1} for the sphere. This is the physiological advantage of the discoidal shape of the human red blood cell.

The results in Fig. 1 show clearly that, regardless of the model chosen, complete stirring does not occur during oxygen uptake by red cells in our stopped-flow mixing apparatus. The observed time courses exhibit rates that are much less than those predicted. Simulation of the situation for no stirring was considerably more difficult and time consuming. We approached the problem by computing time courses with progressively larger unstirred layers until increasing the layer thickness produced no further effect on the resultant time courses. For both three-dimensional models, this was achieved between 20- and 30-μm away from the cell surface (Figs. 1 *A* and *B*). In the case of the one-dimensional plane sheet model, the oxygenation rate continues to decrease in this range and approaches values that are 100 times less than those observed experimentally (Fig. 1 *C*). These results point out dramatically the inadequacy of the plane sheet model when external diffusion is considered (see also Rice, 1980). The problem is a result of the use of only one dimension. For this scheme, computations must go out to a minimum of 120 μm to obtain enough oxygen molecules to saturate the cellular hemoglobin under conditions of no stirring and 0.125 mM external O_2 concentration. For the cylindrical and spherical models, the volume unit containing enough oxygen is contained within a sphere that is ~15 μm in radius surrounding the red cell.

More specific differences between the three models are shown in Fig. 2, where external and internal oxygen gradients and intracellular oxyhemoglobin profiles are displayed. These curves were generated with a fixed 20-μm unstirred layer. For both the spherical and the cylindrical

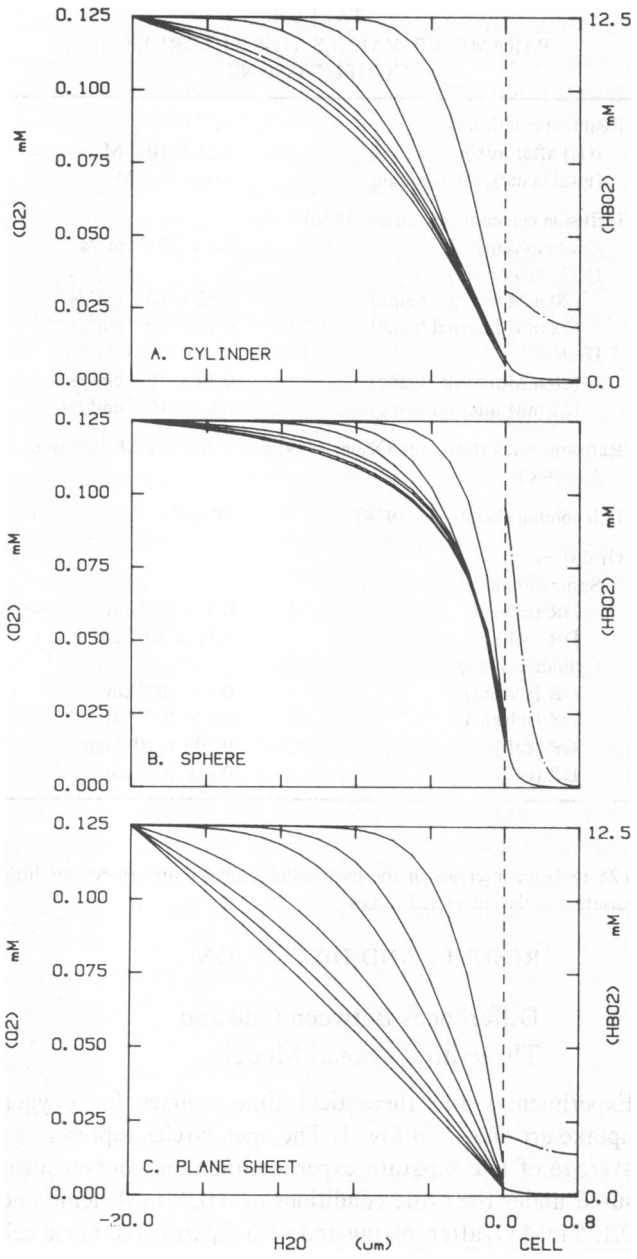

FIGURE 2 Theoretical oxygen concentration profiles (solid lines, —) adjacent to the cell surface at 0, 2, 6, 10, 20, 30, 40, and 60 ms after initiation of the reaction. The oxygen (—) and oxyhemoglobin (— · —) reaction concentrations shown inside the cell were computed for 60 ms after mixing. The dashed line (---) indicates the cell surface. Initial conditions were 0.125 mM O_2 up to the cell surface, 0 mM O_2 and 0 mM HbO_2, intracellularly, and a 20-μm fixed unstirred solvent layer. The other parameters used are given in Table I. (*A*) Cylindrical model with concentration profiles plotted normal to the cell surface along the *z*-axis at $r = 0$. (*B*) Spherical model concentration profiles along the *r*-axis. The distance from the cell surface to the cell center is 2.75 μm for this model, not 0 to 0.8 μm as for the cylinder and plane sheet models. (*C*) Plane sheet model concentration profiles along the *x*-axis.

models, an extracellular, steady-state oxygen gradient is formed within ~10 ms after mixing and remains constant throughout most of the reaction. The differences between the magnitudes of these external gradients are primarily a reflection of the differences between the two geometrical

representations. For the sphere, the oxygen concentration is plotted vs. the radial distance; for the cylinder, the concentration is plotted vs. the z-direction, which is a line normal to the circular face of the disk and in the center ($r = 0$). As expected, the plane sheet model exhibits unrealistic external O_2 concentration profiles (Fig. 2 *C*). No steady-state pattern occurs, and the oxygen concentration gradient approaches zero at the cell surface as the reaction proceeds. For the cylinder a steady-state intracellular oxygen gradient forms after 10 ms, whereas the intracellular gradients are continuously changing in the sphere. The oxyhemoglobin profile at 60 ms after flow has stopped is also very asymmetric for the spherical model; high concentrations of oxyhemoglobin are present adjacent to the cell surface, whereas at the cell center, the concentration is zero. This reflects slow intracellular diffusion for the spherical cell, even in the absence of stirring. A much more uniform oxyhemoglobin pattern is observed for the cylindrical cell.

Evidence for Some Degree of Stirring

The condition of no stirring also does not represent the observed situation (far right curves in Fig. 1). In the case of the plane sheet model, the discrepancy between the observed and calculated time courses is quite large. This result led Coin and Olson (1979) to postulate that stirring still occurred after flow stopped and that the mean unstirred layer during the reaction was 2–3 μm (Fig. 1 *C*). A similar degree of stirring is required to fit the curve for the spherical model to that found experimentally (Fig. 1 *B*). In contrast, fits to the experimental data using the cylindrical disk model suggest much less stirring (Fig. 1 *A*) and the discrepancy between the observed curve and that computed in the absence of mixing is small. A fixed stagnant layer of ~8 μm allows a more quantitative fit to the cylindrical model (Fig. 3). Because the disk is the most accurate representation of the red cell shape, these results raise the question as to whether there is any mixing after flow stops. The results in Figs. 1 *A* and 3 suggest that there is, but to a lesser extent than that predicted previously with either a plane sheet (Coin and Olson, 1979) or a spherical model (Huxley and Kutchai, 1983).

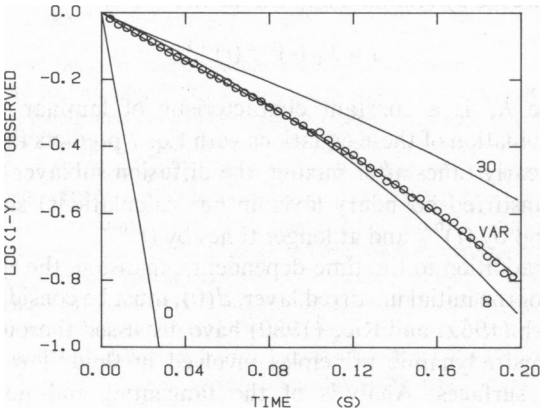

FIGURE 3 Comparisons of the experimental time course with those computed for the fixed and variable unstirred layer, cylindrical models. The open circles (O) represent the experimental observations (see Fig. 1). The solid lines (—) represent the various theoretical curves. Fixed layer thicknesses are given in microns and *VAR* refers to the theoretical model calculated from the expansion of the unstirred layer according to Eq. 10.

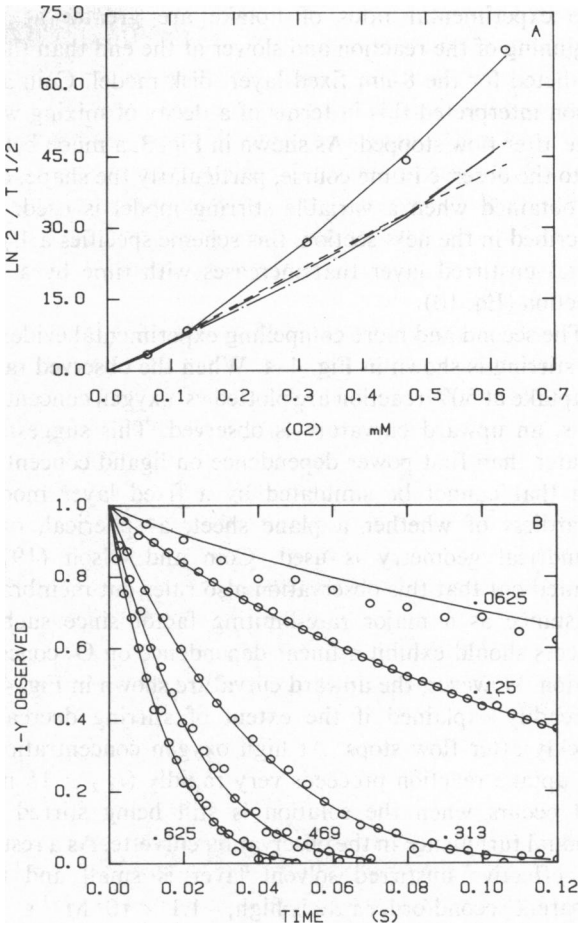

FIGURE 4 Dependence of the rate of oxygen uptake by red cells on oxygen concentration. Open circles (O) represent observed oxygen uptake rates for deoxygenated red cells (22 mM internal heme). Reaction conditions were: 0.020 mM total heme and 0.0625, 0.125, 0.313, 0.469, and 0.625 mM O_2 after mixing. The solid lines (—) in both panels represent rates for time courses computed with a cylindrical model that incorporates the variable unstirred layer formulation given by Eq. 10. (*A*) Dependence of the observed rate (ln 2/half-time) on oxygen concentration. — — —, rates calculated using the cylindrical model with a fixed 8-μm unstirred layer; - - -, rates calculated using the spherical model with a fixed 2-μm unstirred layer; — · —, rates calculated using the plane sheet model with a fixed 2.5-μm unstirred layer. (*B*) Experimental (open circles, O) and theoretical (solid lines, —) time courses at the various oxygen concentrations given in millimoles per liter beside each curve.

Two other observations suggest that stirring does take place in our stopped-flow experiments. The first is that the shape of the experimental time course cannot be simulated exactly by a fixed unstirred layer model. Coin and Olson (1978) pointed this out using the one-dimensional plane sheet model, and as shown in Fig. 3, this discrepancy still occurs when the more realistic cylindrical model is used.

The experimental rates of uptake are greater at the beginning of the reaction and slower at the end than those predicted for the 8-μm fixed layer, disk model. Coin and Olson interpreted this in terms of a decay of mixing with time after flow stopped. As shown in Fig. 3, a much better fit to the observed time course, particularly the shape, can be obtained when a variable stirring model is used. As described in the next section, this scheme specifies a 1-μm initial unstirred layer that increases with time by a $t^{1/2}$ function (Eq. 10).

The second and more compelling experimental evidence for stirring is shown in Fig. 4 *A*. When the observed rates of uptake at 50% reaction are plotted vs. oxygen concentrations, an upward curvature is observed. This suggests a greater than first power dependence on ligand concentration that cannot be simulated by a fixed layer model, regardless of whether a plane sheet, a spherical, or a cylindrical geometry is used. Coin and Olson (1979) pointed out that this observation also rules out membrane resistance as a major rate-limiting factor since such a process should exhibit a linear dependence on O_2 concentration. However, the upward curvature shown in Fig. 4 *A* is readily explained if the extent of stirring decreases quickly after flow stops. At high oxygen concentrations, the uptake reaction proceeds very rapidly ($t_{1/2} \leq 15$ ms) and occurs when the solution is still being stirred by residual turbulence in the observation curvette. As a result, the effective unstirred solvent layer is small and the apparent second-order rate is high, $\sim 1.1 \times 10^5$ M^{-1} s^{-1} at 0.625 mM O_2. At lower oxygen concentrations, when the overall reaction proceeds much more slowly ($t_{1/2} \geq 80$ ms), there is very little residual stirring and the apparent second-order rate is significantly smaller, 0.54×10^5 M^{-1} s^{-1} at 0.0625 mM O_2. These effects can be simulated using the variable unstirred layer scheme described in the next section, and, as shown in Fig. 4 *B*, this cylindrical model can account quantitatively for both the observed rates and the shapes of the time courses at various oxygen concentrations.

Theories for Stirring and Its Decay with Time

Mixing in fluids during either laminar or turbulent flow can be considered in terms of the movement of small volume elements or eddies (Levich, 1962; Bird et al., 1960; and Rice, 1980). The size of these elements is determined by the rate of bulk fluid flow, the kinematic viscosity of the fluid, and the geometry of the flow device. In the stopped-flow apparatus, the reactant solutions are mixed at high Reynold's numbers and then flow is abruptly halted. Even after net flow has been interrupted, a substantial amount of residual eddy turbulence takes place. Gad-el-Hak et al. (1977) measured the length of these microscale eddies in red cell suspensions using an apparatus similar to ours and laser anemometry. The microscale lengths, l, were 10 times larger than the diameter of the cells, $l \simeq 80$ μm, and increased in size as the initial turbulence decayed. Thus, each erythrocyte can be considered located within a viscous layer of fluid that extends out ~70–90 μm from the cell surface. This large viscous sublayer is related but not directly equal to the much smaller unstirred boundary layer used in our theoretical computations.

Levich (1962) has pointed out that the eddy sizes and shapes are continuously changing, and only mean values are observed. Solute is transferred across most of the viscous sublayer by turbulence (i.e., volume transfer between the fluid elements). Molecular diffusion only becomes the dominant mechanism of mass transport very near the cell surface. According to Levich (1962) and Rice (1980), the thickness of this diffusion sublayer, d, can be calculated from

$$d = (R)^{1/3}\, l^{2/3}\, (Pr)^{-1/3}, \tag{7}$$

where R is the radius of the erythrocyte, l is the microscale eddy length, and Pr is the Prandtl number, which is the ratio of the kinematic viscosity for fluid flow, ν, to the molecular diffusion constant, D, of the solute in question. Using Gad-el-Hak et al.'s (1977) value of 80 μm for l, R = 4 μm, $D = 2.1 \times 10^{-5}$ cm^2/s for O_2, and $\nu = 0.01$ cm^2/s, Eq. 7 predicts a thickness of ~4 μm for the diffusion sublayer at times shortly after flow has stopped in our experiments.

The increase in length of the viscous sublayer with time after flow stops can be estimated from consideration of the equations for energy dissipation in fluid flow (Rice, 1980). At early times during turbulent flow, Landau and Liftschitz (1959) have suggested that the microscale length increases according to the following time dependence

$$l = K_T\, (\nu)^{3/4}\, (t)^{17/28}, \tag{8}$$

where K_T is an undefined proportionality constant for the turbulent flow situation. At longer times during laminar flow, the thickness of the viscous sublayer was postulated to increase by (Landau and Liftschitz, 1959)

$$l = K_L\, (\nu)^{11/8}\, (t)^{7/8}, \tag{9}$$

where K_L is a constant characteristic of laminar flow. Combination of these equations with Eq. 7 predicts that at very early times after mixing, the diffusion sublayer (i.e., the unstirred boundary layer in our calculations) should expand by $(t)^{0.41}$ and at longer times by $(t)^{0.58}$.

In addition to the time-dependent expansion, the thickness of the initial unstirred layer, $d(0)$, must be considered. Levich (1962) and Rice (1980) have discussed thoroughly the hydrodynamic principles involved in fluid flow past solid surfaces. Analysis of the tangential and normal velocity components of the fluid at the cell surface prescribes a motionless layer of solvent that exists at the cell surface even during turbulent flow. Rice (1980) has estimated that the initial diffusion sublayer is ~1–2 μm under the mixing conditions in the conventional stopped-flow apparatus.

The general form for the time dependence of the expansion of the unstirred sublayer is

$$d(t) = d(0) + K(t)^A, \quad (10)$$

where $d(t)$ is the thickness of the unstirred layer (i.e., the distance from the cell surface to the outer boundary layer where the oxygen concentration is fixed equal to that in bulk solvent) and K is a proportionality constant whose absolute value must be determined experimentally, but whose dependence on viscosity can be computed by combining Eqs. 7 through 10. The assignment of numerical values to $d(0)$, K, and A was an iterative procedure. The final values used to fit the rate data and time courses in Figs. 3–5 were: $d(0) = 1 \times 10^{-4}$ cm, $K = 0.0041$ cm $s^{-1/2}$, and $A = 0.5$. Time courses computed using $d(0)$ equal to 0, 1, and 2×10^{-4} cm are very similar (Fig. 5). We chose a 1-μm initial unstirred layer as the most reasonable value based on the theoretical considerations of Rice (1980).

A comparison of four expressions for the expansion of the diffusion sublayer with time is shown in Fig. 6. The dashed line represents the empirical exponential formulation described by Coin and Olson (1979)

$$d(t) = d_f(1\text{-}e^{-k_f t}) + d_s(1\text{-}e^{-k_s t}). \quad (11)$$

The subscripts f and s refer to the fast and slow light scattering changes that Coin and Olson (1979) observed when red cells were mixed with buffer in the stopped flow apparatus. The rates for these phases were $k_f = 300\ s^{-1}$ and $k_s = 9\ s^{-1}$. Sets of oxygen uptake time courses were fitted to the cylindrical disk model using Eq. 11 to describe the expansion of the unstirred layer with time; the best-fit values were $d_f = 4$ μm and $d_s = 16$ μm. The remaining three curves in Fig. 6 were computed from Eq. 10 using $d(0) = 1 \times 10^{-4}$ cm and $A = 0.41$, 0.50, or 0.58. At short times after mixing ($t \leq 6$ ms), there are substantial differences between the theories. As pointed out by Rice (1980), the exponential expression does not adequately represent the hydrodynamic events that occur during mixing and immediately after flow stops (Fig. 6 *A*). However, at longer times ($10 < t < 200$ ms), the various expressions, including Eq. 11, are virtually indistinguishable (Fig. 6 *B*). All of them can be used to accurately simulate the data in Fig. 4. The dead-time of the stopped-flow apparatus is 6 ms under our conditions, which maximize flow rates and minimize cell lysis (Coin and Olson, 1979, and Coin, 1979). Thus, the differences between the theories at short times are not apparent in the computed time courses. We selected a value of 0.5 for A because it represents the mean value for the exponent when comparing the turbulent (Eq. 8) and laminar (Eq. 9) flow expansion theories. Again, there is very little difference between these theories on the time scales used experimentally, and the formulation of a time-dependent expression for A did not seem justified.

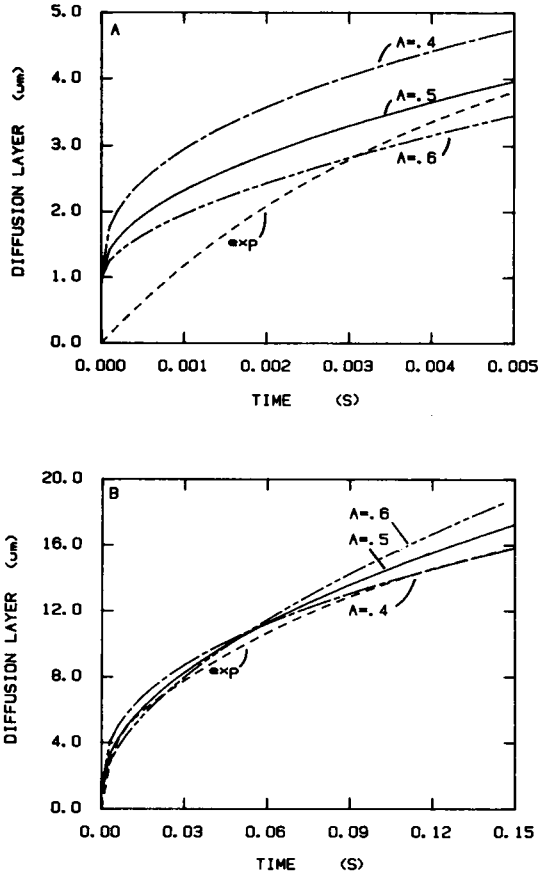

FIGURE 6 Dependence of the thickness of the diffusion sublayer on time after mixing. - - -, the two exponential function calculated from Eq. 11; — - - —, the expansion of the layer calculated from Eq. 10, $D(0) = 1.0 \times 10^{-4}$ cm, $K = 0.0041$ cm $s^{-1/2}$, and $A = 0.58$; ——, the expansion using Eq. 10, the same $D(0)$ and K parameters, and $A = 0.5$; — · —, the expansion using Eq. 10, the same $D(0)$ and K parameters, and $A = 0.41$. (*A*) The expansion of the diffusion layer over a short time period (<6 ms). This occurs within the dead time of the stopped-flow apparatus. (*B*) The expansion of the diffusion layer during longer times (0–150 ms).

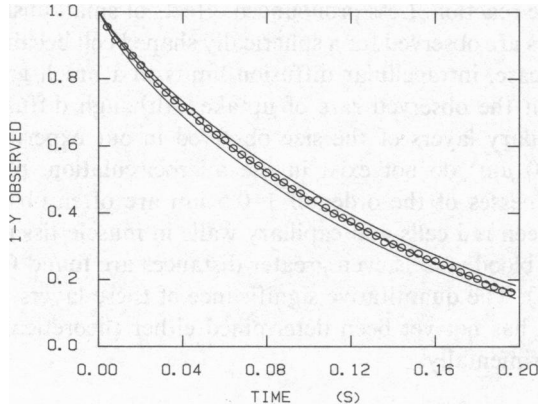

FIGURE 5 Comparison of the experimental time course with theoretical curves computed for oxygen uptake with differing initial unstirred layers ($d[0]$ in Eq. 10). The experimental data (open circles, O) were taken from Fig. 1. The solid lines (——) represent theoretical time courses calculated using the cylindrical, variable unstirred layer model defined in Eq. 10. The value of $d(0)$ was 0, 1, and 2 μm, respectively, for the three curves, left to right; $A = 0.5$; $K = 0.0041$ cm $s^{-1/2}$.

CONCLUSIONS

The three-dimensional cylindrical scheme, which employs Eq. 10 to describe the decrease in stirring with time, exhibits fits to the experimental oxygen uptake data that are as good as those reported previously by Coin and Olson (1979) who used a simpler, more empirical model (Fig. 4). The basic conclusion remains the same. A major rate-limiting process for the reaction of oxygen with erythrocytes in the stopped-flow apparatus is diffusion through stagnant solvent layers, which are adjacent to the red cell surface. The differences between this and the earlier work are quantitative in nature. Coin and Olson (1979) postulated unstirred layers of the order of 2-5 μm during the major portion of the uptake time courses. Similar values were postulated by Rice (1980) and Huxley and Kutchai (1983) using spherical models. The more realistic cylindrical model indicates that there is much less turbulent mixing after flow stops and that the diffusion sublayer is between 8-20 μm during most of the reaction (Fig. 6 *B*).

The time-dependent expression for the unstirred layer given in Eq. 10 can also be used to predict the rates of oxygen uptake by cells suspended in more dense media. The dependence of K in Eq. 10 on external viscosity can be estimated by combining this expression with Eq. 7 and Landau and Liftschitz's expression for the expansion of the microscale length with time during laminar flow (Eq. 9). The latter equation was chosen over the expression for turbulent flow since the laminar stage and its decay predominates during the experimental observations. The resultant dependence on solvent viscosity is given by

$$K = K'_L R^{1/3} (D)^{1/3} (\nu)^{7/12}, \qquad (12)$$

where K'_L is an empirical, proportionality constant derived from Eqs. 7 and 9 (i.e., $K'_L = [K_L]^{2/3}$) and can be evaluated from the fitted value of K and the known values of D (2.1×10^{-5} cm^2) and ν (0.01 cm^2/s) for the reactions in phosphate buffer. Under these conditions, K'_L equals 28.4 cm$^{-7/6}$ s$^{5/12}$. Coin and Olson (1979) carried out a set of O_2-uptake experiments in the presence of 10% bovine serum albumin (BSA) to assess the influence of external viscosity, but did not analyze the results in terms of changes in the degree of stirring. These results can now be analyzed quantitatively and the results of simulations using the cylindrical model and Eqs. 10 and 12 are shown in Fig. 7. The added serum albumin increases the solvent viscosity by a factor of 1.5 (Hatscheck, 1928). The value of D in 10% albumin has been measured independently and reported to be 1.6×10^{-5} cm^2/s (Kreuzer, 1970). Using these values for ν and D and the above value for K'_L, K is computed to be 0.0047 cm s$^{-1/2}$. These parameters were then used to calculate expected time courses in 10% serum albumin. As shown in Fig. 7, the agreement between the observed and calculated rates is excellent. The control (0% BSA) experimental rates were also taken from Coin and Olson (1979). The slightly higher observed rates (open circles, Fig. 7 vs. open circles, Fig. 4 *A*) are due to the lower internal hemoglobin concentration (20 mM) of the cells used by Coin and Olson compared with those used in our current work (22 mM). The cylindrical model employing Eq. 10 can fit all of these situations and appears to be a general scheme for use in analyzing a wide variety of different experimental conditions.

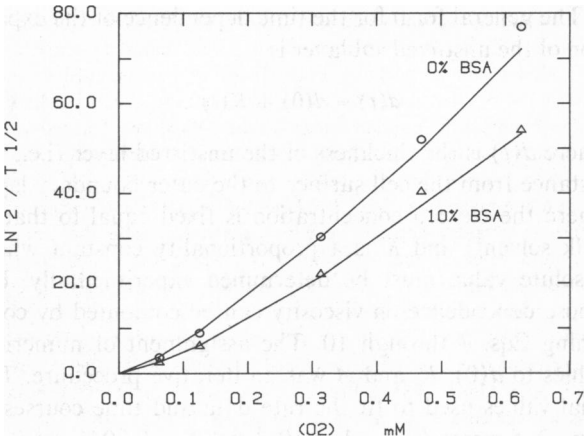

FIGURE 7 Dependence of the rate of oxygen uptake (ln 2/half-time) by red cells on oxygen concentration in the presence (△) and absence (○) of 10% bovine serum albumin (*BSA*). Symbols represent experimental rates taken from Coin and Olson (1979). Reaction conditions are identical to those in our Fig. 1 except for the internal heme concentration of cells used by Coin and Olson (20 mM). The theoretical rates (solid lines, —) were calculated using the cylindrical, variable unstirred layer model as described in the text.

The physiological relevance of unstirred plasma layers during in vivo oxygen uptake and release by erythrocytes is not clear. The results is Fig. 1 *A* show that layers as small as 0.5 to 1.0 μm cause a marked decrease (≥two-fold) in the rate of O_2 uptake by a disk-shaped cell. This effect is exerted on both the initial velocity and the overall half-time of the reaction. Less pronounced effects of small unstirred layers are observed for a spherically shaped cell because, in this case, intracellular diffusion limits to a much greater extent the observed rate of uptake. Although diffusional boundary layers of the size observed in our experiments (8–20 μm) do not exist in the microcirculation, plasma thicknesses of the order of 1–0.5 μm are often observed between red cells and capillary walls in muscle tissues; in liver blood vessels even greater distances are found (Cliff, 1976). The quantitative significance of these layers, however, has not yet been determined either theoretically or experimentally.

APPENDIX

The method of finite differences, as derived from Taylor's theorem, was used to integrate numerically Eqs. 3–6 (see Olson, 1981*b*). With this method, the derivative of a concentration at a point can be approximated by difference quotients over small intervals in both time and space. A three-dimensional grid system was employed to divide the cellular volume

into small intervals. The space intervals, DR for the spherical model and DR and DZ for the cylindrical model, were indexed separately in extracellular and intracellular grids. Indexing was assigned so that i defined the position integer in the r-direction and, for the cylindrical model, j defined the position integer in the z-direction. The cell-solvent interface was defined as 0 for both i and j. Negative integers were used for the solvent layers external to the cell to an outer position, $-NL$, at which the absolute magnitude times DR (and DZ) equals the thickness of the diffusion sublayer. Positive integers were used inside the cell to a maximum value at the cell center, NI, where the system becomes symmetrical (see Fig. 2). The time interval, DT, was indexed by an integer t such that $t * DT$ was equal to the time into the reaction.

The finite-difference equations were solved implicitly using the predictor-corrector technique, first developed by Moll (Moll, 1969; Coin and Olson, 1979; Olson, 1981*b*). Predicted values of O_2 and HbO_2 concentrations were calculated according to the change in their concentrations in the preceding time step. The corrected concentration at the point $C(i[j],t)$ was solved for in terms of the calculated concentration at that point in the previous time interval $C(i,[j],t-1)$ plus a complicated term involving the predicted concentration values at finite-difference points and the chemical-reaction rate parameters. The resultant corrected values of oxygen and hemoglobin concentration were compared with the original predicted values and if the differences exceeded a predefined test value, the equations were reiterated using the corrected concentrations for new predicted values. This iterative process was continued until the differences between the newly calculated concentrations and the predicted concentrations were smaller than test values of 10^{-6} M for O_2 concentrations and 10^{-4} M for HbO_2 concentrations.

Boundary Conditions

Adaptations of the general finite-difference equations were required to describe the diffusion processes at the three boundaries of the models: the outer edge of the extracellular diffusion sublayer, the cell-solvent interface, and the cell center (see Fig. 2).

Edge of the Unstirred Layer. The position in the unstirred layer is specified by the r- and z-axis indices i and j that go from 0 to $-NL$ in the extracellular fluid. The integer NL is defined as $d(t)$ (see Eq. 10, main text) divided by DR or DZ, the grid sizes for the r- and z-directions. At the grid point $-NL$, the concentration of oxygen is fixed equal to the bulk solvent concentration, C_o. In the spherical model only one equation is required for this boundary, whereas for the cylinder, both the z- and r-surfaces of the unstirred layer need to be specified

$$\text{Sphere: } C(i = -NL,t) = C_o \tag{13}$$

$$\text{Cylinder: } C(i = -NL, j = NI \text{ to } -NL,t) = C_o$$
$$C(i = NI \text{ to } -NL, j = -NL,t) = C_o. \tag{14}$$

Oxygen Diffusion at the Cell-Solvent Interface. The boundary condition at the cell surface requires special treatment because this interface separates two diffusionally distinct phases. The techniques for deriving an expression for $\partial c/\partial t$ at this boundary have been described in detail by Crank (1975) and Smith (1978). The flux at the interface can be calculated in terms of oxygen either leaving the solvent phase (s) or entering the cell cytoplasm (c); these fluxes must be equal

$$F(O,t) = D_c \frac{\partial C_c}{\partial R} = D_s \frac{\partial C_s}{\partial R}. \tag{15}$$

In addition, the rates of change of oxygen concentration calculated using either intra- or extracellular concentrations must be equal. For spherical coordinates this requires the following equality

$$\frac{\partial C(O,t)}{\partial t} = D_C \left[\frac{\partial^2 C_c}{\partial R^2} + \frac{2}{R} \frac{\partial C_c}{\partial R} \right] - k' C_c(\text{Hb}) + k(\text{HbO}_2) = D_s \cdot \left[\frac{\partial^2 C_s}{\partial R^2} + \frac{2}{R} \frac{\partial C_s}{\partial R} \right]. \tag{16}$$

Central difference formulas were used to approximate the first derivatives $\partial C_c/\partial R \sim D_c[C_c(+1,t) - C_c(-1,t)]/2DR_c$ and $\partial C_s/\partial R = D_s[C_s(+1,t) - C_s(-1,t)]/2DR_s$. This requires the assignment of values to an "imaginary" cellular oxygen concentration, $C_c(-1,t)$, which is located one grid point outside of the cell and to an "imaginary" solvent oxygen concentration, $C_s(+1,t)$, which is located one grid point inside the cell. This problem also occurs when approximating the cellular and solvent second-order derivatives in Eq. 16 (i.e., $\partial^2 C_c/\partial r^2 = [C_c(+1,t) - 2C_c(O,t) + C_c(-1,t)]/DR_c^2$ and $\partial^2 C_s/\partial r^2 = [C_s(+1,t) - 2C_s(O,t) + C_s(-1,t)]/DR_s^2$). In general, the solubility of oxygen in the two phases need not be the same (see Coin and Olson, 1979; Crank, 1975); however, in all the models presented here $C_c(O,t) = C_s(O,t)$, and there is no need to consider the subscripts. The conditions of equal flux and equal rates of change allow the assignment of values to the imaginary concentrations (i.e., Eqs. 15 and 16 represent simultaneous equations in the two unknowns, $C_c[-1,t]$ and $C_s[+1,t]$). The final boundary equation is obtained by incorporating the values for these concentrations into the general finite difference formula. The resultant formula for the spherical model is

$$\frac{C(0,t) - C(0,t-1)}{DT} = 2 \cdot \frac{DO2_c}{DR_c} \cdot \frac{(1 - DR_s/R) \cdot [C(+1,t) - C(0,t)]}{[DR_s(1 + DR_c/R) + DR_c(1 - DR_s/R)]} + 2 \cdot \frac{DO2_s}{DR_s} \cdot \frac{(1 + DR_c/R)[C(-1,t) - C(0,t)]}{[DR_s(1 + DR_c/R) + DR_c(1 - DR_s/R)]} + DR_c \cdot (1 - DR_s/R) \cdot \frac{\{kG(0,t) + C(0,t) \cdot -k'[G_T - G(0,t)]\}}{[DR_s(1 + DR_c/R) + DR_c(1 - DR_s/R)]}, \tag{17}$$

where $C(i,t)$ equals the concentration of O_2 at point i and time t, $G(i,t)$ equals the concentration of HbO_2, GT equals the total concentration of heme in the cell, and DO_2 equals the oxygen diffusion constant.

The situation for the cylindrical model is more complex primarily because of the need to consider two grid spaces. The appropriate expressions for $\partial C/\partial t$ at the cell surfaces are derived as in the spherical case by using Eq. 15 and the cylindrical equivalent of Eq. 16 (see Eq. 5 of the main text) to obtain assignments for the imaginary intra- and extracellular concentration terms. The major complication is algebraic since approximations for two second-order derivatives must be considered, $\partial^2 C/\partial r^2$ and $\partial^2 C/\partial z^2$. In addition, five separate equations must be derived to represent the following surface conditions. (*a*) At the center of the circular face of the disk, $C(i = NI, j = O,t)$, imaginary cell and solvent concentrations must be obtained for the z-direction (i.e., $C_c[NI,-1,t]$ and $C_s[NI,+1,t]$). Also at this point the special approximations for $\partial C/\partial r$ and $\partial^2 C/\partial r^2$ at the cell center must be employed (see the section entitled Oxygen and Hemoglobin Diffusion at the Cell Center). (*b*) Along the circular face, the rate of change of $C(i = 1 \text{ to } NI - 1, j = O,t)$ is derived using imaginary concentrations in the z-direction and the normal finite difference approximations in the r-direction. (*c*) At the outer edge of the cell (i.e., $i = O, j = O$), imaginary concentrations must be solved for in

both the z- and r-directions. (*d*) Along the short cylindrical surface, the rate of change of $C(i = O, j = 1$ to $NI - 1,t)$ is obtained using imaginary concentrations in the r-direction and the standard finite difference approximation in the z-direction. (*e*) At the center of the short cylindrical surface (i.e., $i = O, j = NI$), imaginary concentrations in the r-direction are obtained and the approximation for ∂^2C/∂^2Z at the cell center is used (see the next section below).

Hemoglobin Diffusion at the Cell-Solvent Interface. When the finite difference formula are applied to hemoglobin diffusion at the cell surface, imaginary external protein concentrations must be considered. In this case, because the protein cannot diffuse across the plasma membrane, the flux at the cell surface must be zero. For the spherical model this condition is represented by the following central difference approximation

$$\frac{\partial G(O,t)}{\partial r} = O \simeq \frac{G_c(+1,t) - G_c(-1,t)}{2DR_c}. \quad (18)$$

This indicates that the imaginary concentration, $G_c(-1,t)$, must equal $G_c(+1,t)$, and the latter can be substituted into the general finite difference formula. The condition of zero flux is also used to assign imaginary extracellular hemoglobin concentrations in the cylindrical model. Again, five separate sets of equations need to be considered in order to describe the situation along the cylindrical disk surface.

Oxygen and Hemoglobin Diffusion at the Cell Center. At the cell center the $(1/r) \cdot (\partial C/\partial r)$ terms in Eqs. 3 through 6 of the main text become indeterminate since both r and $\partial C/\partial r$ are equal to 0. This can be alleviated by considering the Maclaurin expansion of $\partial C/\partial r$ (Smith, 1978): $c'(r) = c'(0) + rc''(0) + 1/2\, r^2C'''(0) + \ldots$. Because the value of $c'(0)$ is zero due to symmetry, the limiting value of $\partial C/\partial r$ is $r\partial^2C/\partial r^2$ so that $(1/r) \cdot \partial C/\partial r \simeq \partial^2C/\partial r^2$ as r approaches zero. Thus, at r equals zero, the terms in the brackets in Eqs. 3–6 simplify to $3\partial^2C/\partial r^2$ for the spherical model and $2\partial^2C/\partial r^2 + \partial^2C/\partial Z^2$ for the cylindrical scheme. The finite difference formula are further simplified by the condition of zero flux that requires the following equalities: for the spherical model, $C(NI + 1,t) = C(NI - 1,t)$, and for the cylindrical model, $C(i = NI + 1,j,t) = C(i = NI - 1,j,t)$ for all values of j, and $C(i,j = NI + 1,t) = C(i,j = NI-1,t)$ for all values of i. Similar equations and equalities apply for the evaluation of hemoglobin concentrations at the cell center.

Calculations of Fractional Saturation

The fractional degree of saturation of the hemoglobin molecules within each cell was computed by dividing the volume weighted average of the grid point oxyhemoglobin concentrations by the total internal heme concentration. For the spherical model, each volume element is defined as a shell with outer and inner radii defined by $R(i)$ and $R(i + 1)$, respectively. The fractional volume of this shell, $V(i)$, is defined as $(4/3)\, \pi\, [R(i)^3 - R(i + 1)^3]/V_{Total}$; where V_{Total} is the total volume of the sphere. The oxyhemoglobin concentration in this shell is defined as the surface area weighted average of the concentrations at i and $i + 1$: $GAV(i,t) = [R(i)^2 \cdot G(i,t) + R(i + 1)^2 \cdot G(i + 1,t)] / [R(i)^2 + R(i + 1)^2]$. The fractional saturation at a given time point is then defined as

$$Y(t) = \left[\sum_{i=0}^{NI-1} V(i) \cdot GAV(i,t)\right] / HIN, \quad (19)$$

where HIN is the total internal heme concentration, usually 22 mM.

A similar procedure is used in the cylinder model. In this case, a cylindrical volume shell is considered. The circumference averaged oxyhemoglobin concentrations are computed between $R(i)$ and $R(i + 1)$ and averaged linearly in the z-direction to obtain a $GAV(i,t)$ value

$$GAV(i,t) = \frac{R(i)\sum_{j=0}^{NI} G(i,j,t) + R(i+1)\sum_{j=0}^{NI} G(i+1,j,t)}{NI \cdot [R(i) + R(i+1)]}. \quad (20)$$

The volume fraction of the cylindrical shell defined between i and $i + 1$ is: $V(i) = \pi\, (R(i)^2 - R(i + 1)^2) \cdot ZH/V_{Total}$, where ZH is the half thickness (height) of the cell in the z-direction and V_{Total} is half the volume of the disk. The fractional saturation of hemoglobin is then computed from Eq. 19.

To compare the theoretical time courses with those obtained experimentally, the 6-ms dead time of the stopped-flow apparatus must be considered. The simplest procedure involves normalizing the observed absorbance changes and defining these values as $1 - Y_{obs} = \Delta A_t / \Delta A_o$. ΔA_t is the absorbance change at any time, and ΔA_o is the total absorbance change that was observed (i.e., the absorbance after flow stops ($t = 0.006$ s after mixing) minus that obtained after the reaction is complete). The definition as $1 - Y_{obs}$ is to indicate that the measured absorbance decrease is a decrease in fractional amount of deoxyhemoglobin. The theoretical calculations generate time courses of $Y(t)$, the fractional amount of oxyhemoglobin vs. time. To compare the computed results with the fractional absorbance changes, the total saturation change between 6 ms and infinite time must be computed, $Y(t = \infty) - Y(t = 0.006)$. This value is used to normalize the remaining fractional saturation changes so that the final equation for presenting the theoretical time courses is

$$1 - Y_{obs} = \frac{Y(t = \infty) - Y(t)}{Y(t = \infty) - Y(t = 0.006)}. \quad (21)$$

The value of $Y(t = \infty)$ can be obtained by extending the calculations for long times but is more readily computed from the appropriate binding equation using the constants in Table I. In these studies we have not taken into account cooperative ligand binding to hemoglobin. Coin and Olson (1979) and others have shown that this is not a problem when simulating oxygen uptake curves at high O_2 concentrations, where $Y(T = \infty) \geq 0.9$. However, at lower oxygen concentrations the discrepancy between $Y(t = \infty)$ calculated using a simple, one step binding model and the observed value becomes significant. Normalizing the time courses as in Eq. 21 only partially alleviates the situation. This problem probably accounts for the difficulty in fitting the observed curve at 0.0625 mM O_2 in Fig. 5 *B*. At the other oxygen concentrations, $Y(t = \infty)$ is always >0.9.

This research was supported by U. S. Public Health Service Grant HL-16093, by Grant C-612 from the Robert A. Welch Foundation, and by a Teacher Scholar Award from the Camille and Henry Dreyfus Foundation (J. Olson). K. Vandegriff is a recipient of a graduate fellowship from the National Institutes of Health Training Grant GM-07833 from the National Institutes of Medical Science.

Received for publication 4 February 1983 and in final form 17 August 1983.

REFERENCES

Battino, R., F. D. Evans, and W. F. Danforth. 1968. Solubilities of seven gases in olive oil with reference to transport through the cell membrane. *J. Am. Oil Chem. Soc.* 45:830–833.

Bird, R. B., W. E. Stewart, and E. N. Lightfoot. 1960. Transport Phenomena. John Wiley and Sons, Inc., New York.

Cliff, W. J. 1976. Blood Vessels. Cambridge University Press, Cambridge.

Coin, J. T. 1979. The kinetics of oxygen uptake and release by human red blood cells. Ph.D. dissertation, William Marsh Rice University, Houston, TX.

Coin, J. T., and J. S. Olson. 1978. The kinetics of oxygen binding to human red blood cells. *In* Clinical and Biochemical Aspects of Hemoglobin Abnormalities. W. S. Caughey, editor. Academic Press, Inc., New York. 559–576.

Coin, J. T., and J. S. Olson. 1979. The rate of oxygen uptake by human red blood cells. *J. Biol. Chem.* 254:1178–1190.

Crank, J. 1975. The Mathematics of Diffusion. Second ed. Oxford University Press, London.

Fischkoff, S., and J. M. Vanderkooi. 1975. Oxygen diffusion in biological and artificial membranes determined by the fluorochrome pyrene. *J. Gen. Physiol.* 65:663–676.

Forster, R. E. 1964. *In* Handbook of Physiology. W. O. Fenn and H. Rahn, editors. American Physiology Society, Washington, DC, Section 3. 1:827–837.

Gad-el-Hak, M., J. B. Morton, and H. Kutchai. 1977. Turbulent flow of red cells in dilute suspensions. *Biophys. J.* 18:289–300.

Hartridge, H., and F. J. W. Roughton. 1927. The rate of distribution of dissolved gases between the red blood corpuscle and its fluid environment. *J. Physiol. (Lond.).* 62:232–242.

Hatscheck, E. 1928. The Viscosity of Liquids. Van Nostrand Reinhold Co., Inc., New York. 194.

Huxley, V. H., and H. Kutchai. 1981. The effect of the red cell membrane and a diffusion boundary layer on the rate of oxygen uptake by human erythrocytes. *J. Physiol. (Lond.).* 316:75–83.

Huxley, V. H., and H. Kutchai. 1983. Effect of diffusion boundary layers on the initial uptake of O_2 by red cells. Theory vs. experiment. *Microvas. Res.* 26:89–107.

Kagawa, T., and M. Mochizuki. 1982. Numerical solution of partial differential equation describing oxygenation rate of the red blood cell. *Jpn. J. Physiol.* 32:197–218.

Kreuzer, F. 1970. Facilitated diffusion of oxygen and its possible significance; a review. *Respir. Physiol.* 9:1–30.

Kutchai, H. 1975. Role of the red cell membrane in oxygen uptake. *Respir. Physiol.* 23:121–132.

Landau, L. D., and E. M. Liftschitz. 1959. Fluid Mechanics. Pergamon Press, London.

Levich, V. G. 1962. *Physiochemical Hydrodynamics.* Prentice-Hall Inc., Englewood Cliffs, NJ.

Moll, W. 1969. The influence of hemoglobin diffusion on oxygen uptake and release by red cells. *Respir. Physiol.* 6:1–15.

Nicolson, P., and F. J. W. Roughton. 1951. A theoretical study of the influence of diffusion and chemical reaction velocity on the rate of exchange of carbon monoxide and oxygen between the red blood corpuscle and the surrounding fluid. *Proc. Roy. Soc. Lond. B. Biol. Sci.* 138:241–264.

Olson, J. S. 1981*a*. Stopped-flow, rapid mixing measurements of ligand binding to hemoglobin and red cells. *Methods Enzymol.* 76:631–651.

Olson, J. S. 1981*b*. Numerical analysis of kinetic ligand binding data. *Methods Enzymol.* 76:652–667.

Rice, S. A. 1980. Hydrodynamic and diffusion considerations of rapid-mix experiments with red blood cells. *Biophys. J.* 29:65–78.

Roughton, F. J. W. 1932. Diffusion and chemical reaction velocity as joint factors in determining the rate of uptake of oxygen and carbon monoxide by red blood corpuscles. *Proc. Roy. Soc. Lond. B. Biol. Sci.* 111:1–36.

Roughton, F. J. W. 1959. Diffusion and simultaneous chemical reaction velocity in hemoglobin solutions and red cell suspensions. *Prog. Biophys. Chem.* 9:55–104.

Smith, G. D. 1978, Numerical Solution of Partial Differential Equations. Second ed. Clarendon Press, Oxford. 1–74.

Weingarden, M., H. Mizukami, and S. A. Rice. 1982*a*. Transient effects on the initial rate of oxygenation of red blood cells. *Bull. Math. Biol.* 44:119–134.

Weingarden, M., H. Mizukami, and S. A. Rice. 1982*b*. Factors defining the rate of oxygen uptake by the red blood cell. *Bull. Math. Biol.* 44:135–147.

Wintrobe, M. M. 1974. Clinical Hematology. Seventh ed. Lea and Febiger, Philadelphia. 91–92.